Gain uniformity optimization of SOA-based optical packet switching nodes for performance and scalability improvements

Benjamin G. Lee,* Caroline P. Lai, Justin D. Foster, Benjamin A. Small, and Keren Bergman

Department of Electrical Engineering, Columbia University, 500 West 120th Street, New York, New York 10027, USA
**Corresponding author: benlee@ee.columbia.edu*

Received May 18, 2007; revised July 9, 2007; accepted July 11, 2007; published August 6, 2007 (Doc. ID 83155)

A design methodology is proposed that can potentially provide effective bandwidth and scalability improvements to optical packet switching environments utilizing semiconductor optical amplifiers as broadcast-and-select switching elements. The design achieves added uniformity in the nodal gain–loss spectrum. The methodology is tested and verified using a commercial device with measurements performed on the gain, noise figure, optical signal-to-noise ratio, and power penalty. © 2007 Optical Society of America

OCIS codes: 060.4250, 060.4510, 250.5980.

1. Introduction

Optical packet switching (OPS) provides attractive solutions to communications bottlenecks in ultra-high-bandwidth interconnection networks by offering a unique combination of enormous transmission capacity and routing versatility [1,2]. Perhaps the greatest advantage lightwave systems provide over other technologies is the bandwidth enabled by wavelength division multiplexing (WDM). Additionally, the increased link utilization offered by packet switched networks further enhances the overall network capacity. OPS networks have recently gained the focus of significant research, and numerous OPS systems have been constructed for research purposes [3–12].

From the perspective of the photonic packet format, OPS systems employing WDM technology can be divided into two distinct categories: (1) those that use single-wavelength packets in which independent data streams, encoded on separate wavelengths and often intended for different destinations, momentarily traverse network elements simultaneously [3–9], and (2) those systems that use multiple-wavelength data structures that traverse network components as a cohesive unit from source to destination [10–12]. A system following the design of the latter case may implement a packet such as the one shown in Fig. 1, where the address information is encoded in single-bit wavelength stripes. Whereas the former case is free to resolve contention in any of the wavelength, time, or space domains, the latter is limited to space- or time-domain contention resolution. Wavelength-striped packet structures present an attractive solution because they directly leverage the full WDM bandwidth advantage of the optical domain. In both categories, however, a single switching node within a particular network should have the same effect on the power and noise properties of every packet within the system, regardless of the packet wavelength(s) or power, and all nodes should behave equivalently in order to facilitate a modular system. Both of these requirements are met when the switching nodes deliver unity gain to each wavelength used in the network and contribute insignificantly to noise degradation. This is a particularly difficult design to realize, however, because it requires wavelength-independent switching elements [13–17]. Nevertheless, by improving the wavelength uniformity of the nodes, the bandwidth and scalability of a network can be increased. Since the number of switching nodes through which a signal must traverse commonly scales with the logarithm of the number of output ports in a net-

1536-5379/07/091055-9/$15.00

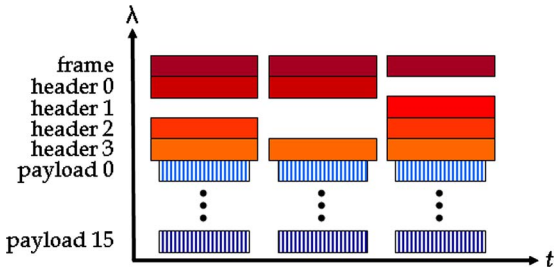

Fig. 1. Example of a multiple-wavelength packet format. This specific format utilizes 16 payload channels alongside five single-bit routing channels [11–13].

work (e.g., Banyan networks [18]), the ability of a packet to traverse a small number of additional hops can significantly increase the allowable network port count.

This paper reports an OPS node design methodology, based on well-known properties of semiconductor optical amplifiers (SOAs), which improves the bandwidth and scalability of multiple-wavelength OPS networks composed of discrete switching nodes. The experimental characterization of a commercial SOA verifies these improvements and explores the effects of the reported design methodology on signal integrity in the switching nodes. We first discuss the structure of one common switching node implementation in Section 2, i.e., the arrangement of SOAs and other fiber-optic components, along with the realistic deviations from the ideal nodes. Then, we show experimentally in Section 3 that SOAs achieve more spectral uniformity when they operate at or near a specific drive current value, unique to an SOA device structure. Sections 4 and 5 evaluate the SOA noise figure and power penalty, respectively, associated with the proposed optimized operating condition. Conclusions are given in Section 6.

2. Switching Node

Many switching node designs have been proposed, but perhaps the most successful schemes incorporate SOAs as wideband switching elements [1,13–17,19–21]. The structure of this kind of SOA-based switching node is straightforward and can demonstrate a high degree of modularity and flexibility. Although there are variations, the basic broadcast-and-select switching node contains a series of couplers for splitting the optical packet to all of the possible output ports, and selects the appropriate destination port by enabling only one or some of the SOA switching elements. Different network architectures and contention resolution mechanisms may require either the single-packet [Fig. 2(a)] or the nonblocking [Fig. 2(b)] switching structures. The nodes offer both simplicity and functionality, and require only a few commonly available fiber-optic components in order to implement a node capable of routing optical data transparently on an ultrafast time scale (approximately nanoseconds). Additionally, the nodes can provide ON–OFF extinction ratios of more than 50 dB [13] due to the large amount of absorption that a signal undergoes as it passes through an SOA in

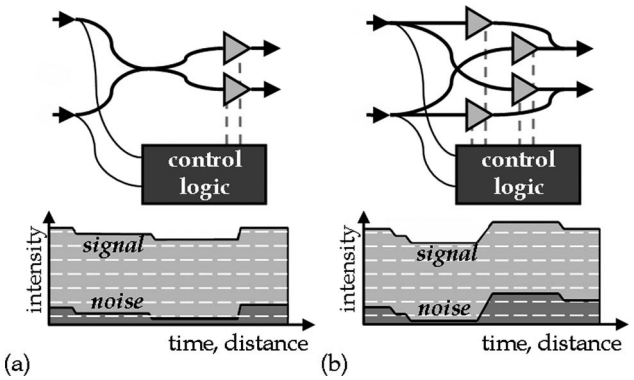

Fig. 2. Schematic (top) and packet power diagram (bottom) of the (a) single packet and (b) nonblocking SOA-based OPS nodes. The optical power can ideally be preserved through the node with only slight additions in noise power. However, the wavelength-dependent gain–loss limits this desired property.

the OFF state. Finally, because the SOAs operate over a wide range of wavelengths, this switching node design can be used to switch packets that are made up of wavelengths spanning more than 50 nm, and can therefore be used in ultra-high-bandwidth networks.

Ideally, the SOA switching element provides the optical signal with amplification to exactly overcome the losses incurred by the first part of the switching node; no net gain or loss should be introduced, satisfying the design requirements outlined previously (Fig. 2). When this condition is met, the switching nodes may be easily cascaded. Of course, some degradation and added noise is incurred as a packet propagates through a switching element. Nevertheless, implementing cascades of these switching nodes is straightforward, and an eight-channel WDM packet has been propagated through a cascade of 58 SOAs with bit error rates (BERs) below 10^{-9} [16].

3. Gain Variance

The robustness of the above switching node design is limited by the curvature of the SOA gain spectrum. Maintaining equal power at the input and output of the node for every wavelength is difficult, because some wavelengths receive more amplification than others [15,16]. As a result, a packet that has propagated through many nodes may simultaneously experience gain saturation in channels located in high-gain regions, inducing interchannel cross talk, and critically low power levels in channels in low-gain regions, leading to optical signal-to-noise ratio (OSNR) degradation [16]. This forces large networks, which send packets through many nodes, to reduce the spectral bandwidth to a small range of wavelengths where the gain variance is tolerable [16]. Conversely, the scalability and bandwidth of a particular network may be expanded by improving the gain uniformity in the SOA switching elements.

One approach, used primarily in long-haul transmission systems utilizing erbium-doped fiber amplifiers (EDFAs), is to add gain compensating filters [22,23]. These filters provide greater attenuation for the wavelengths at which the amplifier produces higher gain. Although this increases the uniformity of the gain spectrum, the approach is not well-suited for packet switched environments because it wastes power, leads to greater noise accumulation, and can require a large number of costly custom-designed components.

A simple, low-cost solution introduced here involves exploiting the inherent properties of the SOA to achieve more gain uniformity. SOAs have previously been explored in depth [24–27]. Some have even discussed the optimization of SOA-based systems, including long-haul in-line amplifier systems [28] and the gain settings for successive amplifiers within a large-scale multistage switch [29]. Here, we leverage the fact that the SOA gain peak shifts toward shorter wavelengths as the drive current is increased [15,27] to propose an SOA operating point (i.e., drive current value) that delivers the most uniform gain spectrum over a specific range of wavelengths. The utilization of this optimal operating point can enhance multiple-wavelength networks by offering a more uniform gain spectrum. Additionally, this technique can be used to minimize the added noise and lost power in systems that also employ gain compensating filters to further flatten the gain spectrum.

An experimental determination of the operating point that minimizes the gain variance has been performed for the A1901 SOA device originally purchased from Alcatel (now Alcatel-Lucent; Murray Hill, NJ). The device measurement sheet for the SOA reports gain and noise figure values of 17.1 and 7.8 dB, respectively, when supplied with a 200 mA drive current at 1550 nm. Although we focus here on only a single device, our methodology for obtaining gain flatness may be extended to systems utilizing other SOAs as well.

The experimental setup for these measurements employs (1) five commercial distributed feedback (DFB) lasers, which operate at constant current and temperature values with outputs multiplexed onto a single fiber, (2) the selected SOA, and (3) an optical spectrum analyzer (OSA). For this experiment, the five signal wavelengths are located along relatively evenly spaced intervals of the ITU *C*-band: 1530.7, 1539.3, 1547.3, 1554.8, and 1563.6 nm. However, the methodology may be tailored to any specific wavelength band that is being used in a given OPS network and is located within the SOA bandwidth. The gain of each channel is recorded for a range of drive currents (Fig. 3), while the SOA is held at constant temperature (25°C). As the current

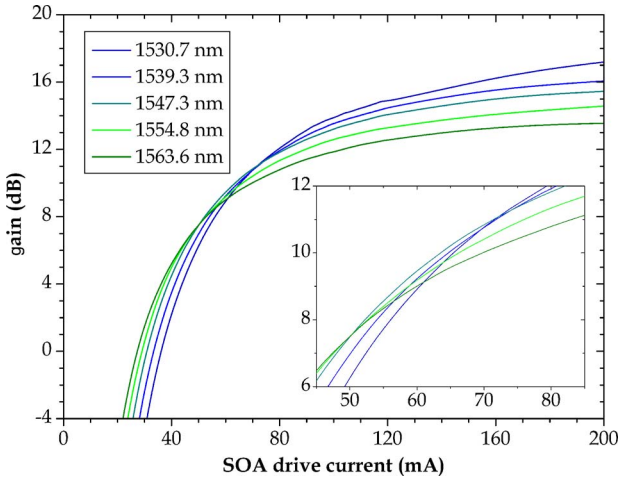

Fig. 3. Gain versus drive current for the Alcatel SOA for the five-wavelength signal with a total packet input power of −13 dBm. The inset zooms in on the optimal operating point.

increases, the wavelength that experiences the highest gain decreases. This is a well-known property of SOAs, and can be further understood by considering the amplified spontaneous emission (ASE) spectra at varying current values (Fig. 4). To correlate with the gain measurements, the ASE spectra have been corrected for the wavelength dependence of the input facet. As the parabolalike gain curve moves across the wavelength band of interest, there is a single operating point that results in the most uniform gain spectrum (occurring between 60 and 70 mA in Fig. 4). Looking back to Fig. 3, the gain variance, defined as the difference in gain between the most- and least-amplified channels, has a minimum value at approximately 62 mA, which indicates our proposed optimal operating point, and yields an average optimized gain of 9.4 dB.

The OPS system design methodology previously discussed implements a constant power solution via unity gain through the switching nodes so that packets at different locations in the network all have equal power levels. However, it is important for the network to robustly manage moderate power fluctuations that will inevitably be introduced. As the SOA input power nears device saturation, the current that is required to reach the optimal setting increases (Fig. 5, red); i.e., the crossing point in Fig. 3 moves to higher current values. Nevertheless, over the range of packet power levels typically used in OPS networks, the optimization current remains very stable. Additionally, by operating in the unsaturated regime, small changes in the power of certain wavelength channels, or the addition or omission of entire wavelength channels, have only slight effects on the gain experienced by other wavelengths. Further, by plotting the gain variance versus input power for a switching node where the SOA is driven with

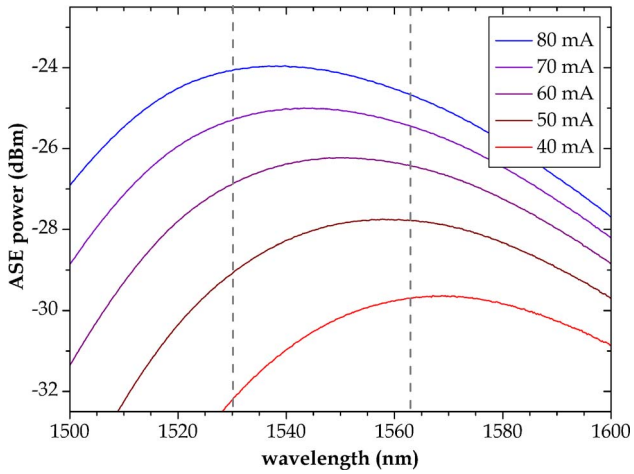

Fig. 4. ASE spectra taken for the Alcatel SOA at varying drive current levels with no optical input. The dashed lines indicate the wavelength band used throughout this study.

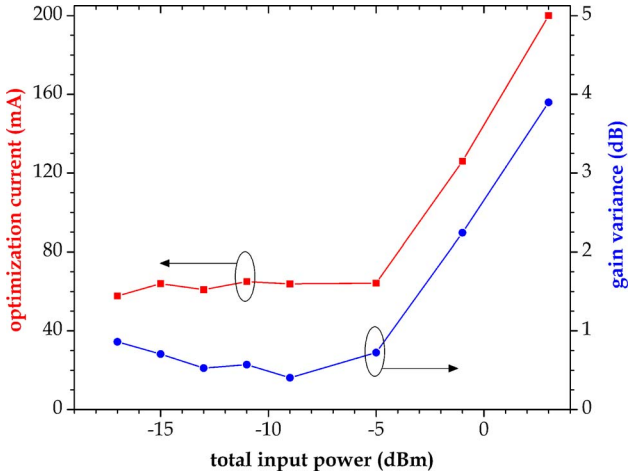

Fig. 5. Input power characteristics of the gain-variance-optimized operating point. The left axis (■) plots the drive current required to minimize gain variance. The right axis (●) plots the measured SOA gain variance at a constant drive current of 62 mA.

a constant drive current of 62 mA (Fig. 5, blue), it is shown that the gain variance across the five wavelengths remains below 1 dB over an input power dynamic range of more than 12 dB, without any adjustments to the node.

4. Noise Figure

Once the gain variance characteristics are determined for a particular SOA, it is important to consider the noise properties associated with the proposed optimized SOA current compared to more standard, high-gain regions of operation. Noise figure is an important metric quantifying the OSNR degradation that a signal experiences when passing through an amplifier. Since the experiment seeks to determine the effect of an SOA on a multiple-wavelength packet, the same five wavelengths used in the gain measurements are inserted into the Alcatel SOA, which is held at a constant temperature (25°C). To determine the noise figure of the SOA, we use the interpolated source-subtraction (ISS) method, which accounts for nonuniformities in the source spontaneous emissions [30]. The optical bandwidth resolution of the OSA for these measurements is 0.06 nm. Near device transparency, small changes in drive current result in large changes in gain. In this region, the noise figure is large and declines sharply with increasing current (Fig. 6). For large current values, variations have a small effect on the device dynamics.

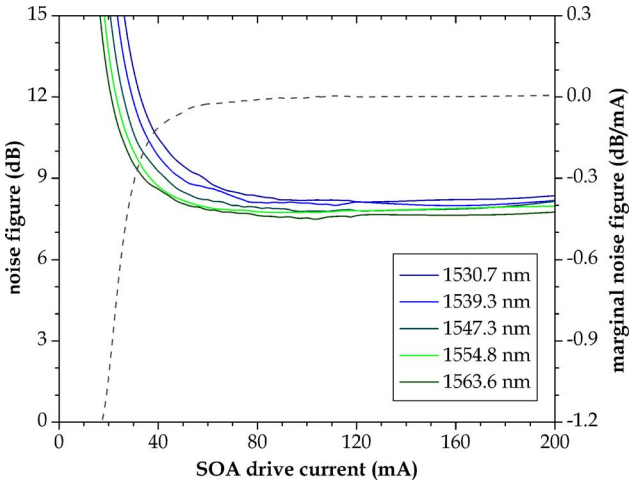

Fig. 6. Noise figure (solid curves) plotted against drive current for each of the five wavelength channels that simultaneously propagate through the SOA with packet input power of −11 dBm. The marginal noise figure (dashed curve) is the numerical derivative of the average noise figure over the five wavelengths.

The marginal noise figure (Fig. 6), defined here as the change in the average noise figure of the five wavelength channels per change in drive current, starts at negative values below device transparency and approaches 0 dB/mA. For drive current values above a threshold value (~60 mA for the Alcatel device at a packet power of −11 dBm), the marginal noise figure is very near to zero, indicating minimal changes in the noise figure at these current values. If the optimal operating current falls below this threshold value, the noise penalty incurred by operating the SOAs at the gain-variance-minimizing current value would be significant. For cases where the optimal current is near or above the threshold, an analysis of the node power penalty should be performed in addition.

5. Power Penalty

Power penalty is a useful metric for determining a system-wide power budget, and is defined as the amount of power required at the receiver to overcome the data errors introduced by the device or by the system under test [31]. The power penalty illustrates how the system will have to be altered by the inclusion (or alteration) of the component. Measurements of the power penalty incurred by multiple-wavelength optical packets propagating through a cascade of SOA-based switch elements are performed using four nodelike structures consisting of a tunable loss element, an SOA, and an isolator, which mitigates backward propagating ASE (Fig. 7). The final node does not include an isolator since no SOA follows it. The statistical variation between the four SOAs is characterized by their gain variance at a common drive current of 64 mA, resulting in 0.5, 0.5, 0.6, and 0.8 dB for the four SOAs. To generate packets, the five-wavelength signal used previously is modulated by a single $LiNbO_3$ modulator with a 2^7-1 pseudorandom bit sequence (PRBS) at 10 Gbits/s in non-return-to-zero (NRZ) format. Then it is decorrelated by more than 20 bits between adjacent wavelength channels in 18 km of single-mode fiber. The modulated signal enters a gating SOA that shapes the data into 25.6 ns packets (32 bytes per wavelength) recurring every 80 ns. The lasers are driven such that the power of the five wavelengths is equalized at the exit of the gating SOA, or likewise entering the first node. For each SOA gain setting explored, the loss elements in the nodes are set so that there is no net gain for the central wavelength channel (1547.3 nm). After the four-node cascade, a packet is directed to a tunable grating filter (λ) and a variable optical attenuator (att). The packet is received by a *p-i-n* photodiode packaged with a transimpedance amplifier and limiting amplifier pair (Rx). The received electronic signal is finally sent to a gated bit-error rate tester (BERT) that is synchronized with the packet gating signal and the bit pattern driven by the pulse pattern generator (PPG). No clock recovery is attempted in this experiment. An optical spectrum analyzer (OSA) and a communications signal analyzer (CSA) are also used for the measurements.

To determine the power penalty, BER measurements are taken and plotted against received power. The BER measurements are taken for the back-to-back case, where the output of the gating SOA is connected directly to the tunable wavelength selector and for three cases where the packet propagates through the four-node cascade. The SOA drive current (and gain of the central wavelength) for the three cases is set to 54 mA (8.0 dB), 64 mA (9.5 dB), and 78 mA (11.0 dB), respectively, representing a measurement below, on, and above the proposed optimal operating point. The power incident on each SOA in the loop is −16 dBm per wavelength (at the central wavelength) in all three sets of measurements. Polarization dependent gain (PDG) is

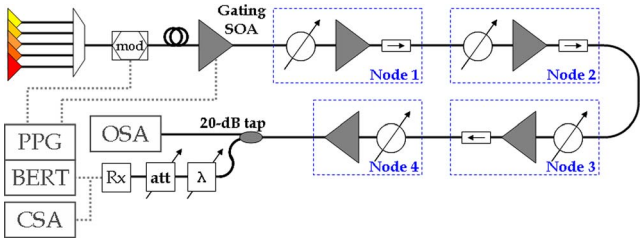

Fig. 7. Experimental setup including a multiple-wavelength packet transmitter, a cascade of four nodelike structures, a receiver, and test and measurement equipment.

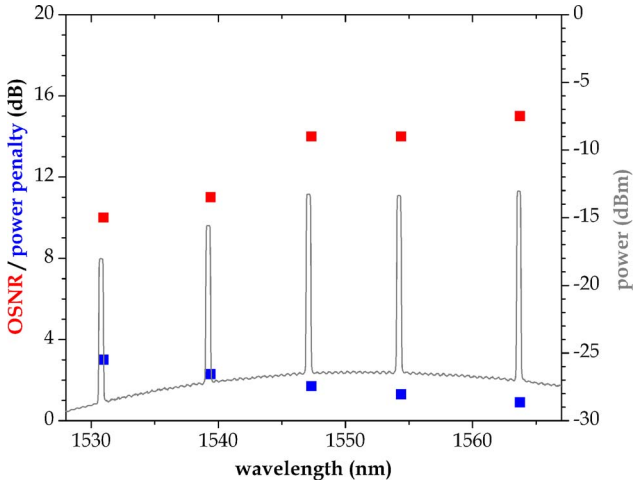

Fig. 8. Power penalty, OSNR, and spectral power with SOA operation lower than the optimized current. Average power penalty is 1.8 dB, and gain variance is 5.0 dB.

apparent in the following results. However, since the OPS nodes introduced earlier do not attempt to address PDG, it would be unwarranted to intentionally avoid it in these experiments, especially since the effects of the drive-current-dependent gain variance far outweigh the observed PDG. These measurements demonstrate an OPS node design methodology; for an analysis of the effects of PDG within SOA-based switching nodes, the readers are directed to [32].

The power penalty trend across the five wavelengths varies for each of the three gain settings (Figs. 8–10). Adjusting the gain below the optimal setting (Fig. 8) results in OSNR degradation, especially for the shorter wavelength channels, because the noise figure is quite large here, as seen in Fig. 6. Even though the power penalty is low at high wavelengths, this is not considered a worthwhile operating point because the gain variance is very large. The measurement implementing the current that provides the optimal gain variance (Fig. 9) is able to maintain high OSNR values at the output of four node hops. In this case, the gain variance is minimized among the three cases with no additional cost to the worst-case power penalty, demonstrating the success of the optimal operating point methodology. Finally, a further increase in gain (Fig. 10), although maintaining high OSNR values, causes increased gain variance across the five wavelengths with no power penalty improvement, marking a strong deviation from the optimal operating point.

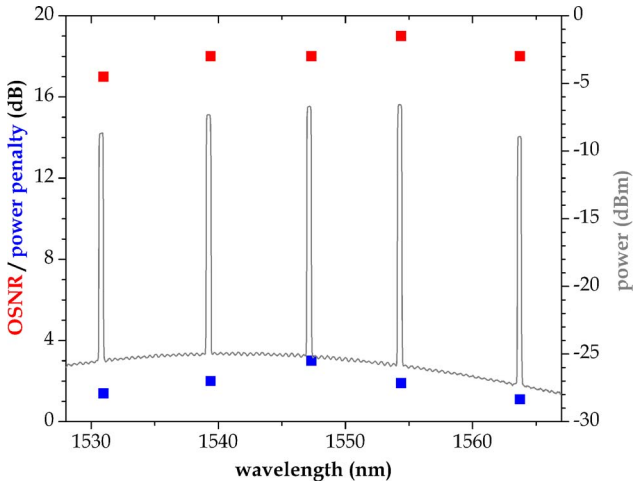

Fig. 9. Power penalty, OSNR, and spectral power with SOA operation at the optimization current. Average power penalty is 1.9 dB, and gain variance is 2.3 dB.

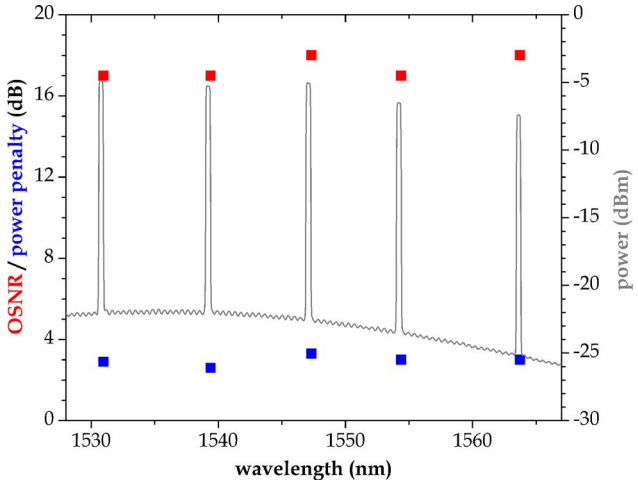

Fig. 10. Power penalty, OSNR, and spectral power with SOA operation higher than the optimized current. Average power penalty is 3.0 dB, and gain variance is 2.5 dB.

6. Conclusions

Here, we have proposed a design methodology that can potentially achieve scalability and effective bandwidth improvements in OPS networks employing SOA-based switching nodes by realizing a node with flatter gain–loss characteristics across a large spectral bandwidth. Well-known properties of SOAs have been used to obtain this gain uniformity, and the proposed design is implemented and tested with commercial SOA devices. We have also evaluated the noise characteristics, and have performed a system-level demonstration of the improvements obtained with the optimized operating point using the commercial device. Other types of SOAs may vary in gain and noise figure, so a detailed investigation should be performed for a given SOA device within a particular network environment following the methodology proposed here. If the gain value associated with the optimal operating current is not well matched to the OPS switching node losses, a small amount of tailoring of the node may improve the fit. For example, extracting more power to the control circuitry in Fig. 2 might improve header recognition and mitigate routing errors. Otherwise, a customized SOA could be designed to suit a specific OPS node implementation.

References and Links

1. R. S. Tucker and W. D. Zhong, "Photonic packet switching: an overview," IEICE Trans. Electron. **E82-C**, 202–212 (1999).
2. G. K. Chang, J. Yu, Y. K. Yeo, A. Chowdhury, and Z. Jia, "Enabling technologies for next-generation optical packet-switching networks," Proc. IEEE **94**, 892–910 (2006).
3. C. Guillemot, M. Renaud, P. Gambini, C. Janz, I. Andonovic, R. Bauknecht, B. Bostica, M. Burzio, F. Callegati, M. Casoni, D. Chiaroni, F. Clérot, S. L. Danielsen, F. Dorgeuille, A. Dupas, A. Franzen, P. B. Hansen, D. K. Hunter, A. Kloch, R. Krähenbühl, B. Lavigne, A. Le Corre, C. Raffaelli, M. Schilling, J.-C. Simon, and L. Zucchelli, "Transparent optical packet switching: the European ACTS KEOPS project approach," J. Lightwave Technol. **16**, 2117–2134 (1998).
4. J. P. Lang, E. A. Varvarigos, and D. J. Blumenthal, "The λ-scheduler: a multiwavelength scheduling switch," J. Lightwave Technol. **18**, 1049–1063 (2000).
5. B. Meagher, G. K. Chang, G. Ellinas, Y. M. Lin, W. Xin, T. F. Chen, X. Yang, A. Chowdhury, J. Young, S. J. B. Yoo, C. Lee, M. Z. Iqbal, T. Robe, H. Dai, Y. J. Chen, and W. I. Way, "Design and implementation of ultra-low latency optical label switching for packet-switched WDM networks," J. Lightwave Technol. **18**, 1978–1987 (2000).
6. R. Hemenway, R. R. Grzybowski, C. Minkenberg, and R. Luijten, "Optical-packet-switched interconnect for supercomputer applications," J. Opt. Netw. **3**, 900–913 (2004).
7. F. Masetti, D. Chiaroni, R. Dragnea, R. Robotham, and D. Zriny, "High-speed high-capacity packet-switching fabric: A key system for required flexibility and capacity," J. Opt. Netw. **2**, 255–265 (2003).
8. F. Xue, Z. Pan, H. Yang, J. Yang, J. Cao, K. Okamoto, S. Kamei, V. Akella, and S. J. B. Yoo, "Design and experimental demonstration of a variable-length optical packet routing system with unified contention resolution," J. Lightwave Technol. **22**, 2570–2581 (2004).
9. S. Rangarajan, H. N. Poulsen, P. G. Donner, R. Gyurek, V. Lal, M. L. Masanovic, and D. J. Blumenthal, "End-to-end layer-3 (IP) packet throughput and latency performance measurements in an all-optical label switched network with dynamic forwarding," in

Proceedings of the Optical Fiber Communication (OFC) Conference 2005 (IEEE, 2005), paper OWC5.
10. D. J. Blumenthal, R. J. Feuerstein, and J. R. Sauer, "First demonstration of multihop all-optical packet switching," IEEE Photon. Technol. Lett. **6**, 457–460 (1994).
11. A. Shacham, B. A. Small, O. Liboiron-Ladouceur, and K. Bergman, "A fully implemented 12×12 data vortex optical packet switching interconnection network," J. Lightwave Technol. **23**, 3066–3075 (2005).
12. A. Shacham, H. Wang, and K. Bergman, "Experimental demonstration of a complete SPINet optical packet switched interconnection network," presented at the Optical Fiber Communication (OFC) Conference 2007, Anabeim, California, 25–29 March 2007, paper OThF7.
13. B. A. Small, A. Shacham, and K. Bergman, "Ultra-low latency optical packet switching node," IEEE Photon. Technol. Lett. **17**, 1564–1566 (2005).
14. J. D. Evankow, Jr. and R. A. Thompson, "Photonic switching modules designed with laser diode amplifiers," IEEE J. Sel. Areas Commun. **6**, 1087–1095 (1988).
15. D. D'Alessandro, G. Giuliani, and S. Donati, "Spectral gain and noise evaluation of SOA and SOA-based switch matrix," IEE Proc.: Optoelectron. **148**, 125–130 (2001).
16. O. Liboiron-Ladouceur, B. A. Small, and K. Bergman, "Physical layer scalability of WDM optical packet interconnection networks," J. Lightwave Technol. **24**, 262–270 (2006).
17. K. A. Williams, G. F. Roberts, L. Tao, R. V. Penty, I. H. White, M. Glick, and D. McAuley, "Integrated optical 2×2 switch for wavelength multiplexed interconnects," IEEE J. Sel. Top. Quantum Electron. **11**, 78–85 (2005).
18. J. A. Hennessey and D. A. Paterson, *Computer Architecture: A Quantitative Approach* (Morgan Kaufmann, 1990), Appendix E.
19. R. Fortenberry, A. J. Lowery, W. L. Ha, and R. S. Tucker, "Photonic packet switch using semiconductor optical amplifier gates," Electron. Lett. **27**, 1305–1307 (1991).
20. C. Tai and W. I. Way, "Dynamic range and switching speed limitations of an $N\times N$ optical packet switch based on low-gain semiconductor optical amplifiers," J. Lightwave Technol. **14**, 525–533 (1996).
21. G. I. Papadimitriou, C. Papazoglou, and A. S. Pomportsis, "Optical switching: switch fabrics, techniques, and architectures," J. Lightwave Technol. **21**, 384–405 (2003).
22. P. F. Wysocki, J. B. Judkins, R. P. Espindola, M. Andrejco, and A. M. Vengsarkar, "Broad-band erbium-doped fiber amplifier flattened beyond 40 nm using long-period grating filter," IEEE Photon. Technol. Lett. **9**, 1343–1345 (1997).
23. C. K. Madsen and J. H. Zhao, *Optical Filter Design and Analysis: A Signal Processing Approach* (Wiley, 1999).
24. N. A. Olsson, "Semiconductor optical amplifiers," Proc. IEEE **80**, 375–382 (1992).
25. M. J. Connelly, *Semiconductor Optical Amplifiers* (Kluwer Academic, 2002).
26. G. Talli and M. J. Adams, "Gain dynamics of semiconductor optical amplifiers and three-wavelength devices," IEEE J. Quantum Electron. **39**, 1305–1313 (2003).
27. A. Bogoni, L. Poti, C. Porzi, M. Scaffardi, P. Ghelfi, and F. Ponzini, "Modeling and measurement of noisy SOA dynamics for ultrafast applications," IEEE J. Sel. Top. Quantum Electron. **10**, 197–205 (2004).
28. M. Settembre, F. Matera, V. Hägele, I. Gabitov, A. W. Mattheus, and S. K. Turitsyn, "Cascaded optical communication systems with in-line semiconductor optical amplifiers," J. Lightwave Technol. **15**, 962–967 (1997).
29. G. Jeong and J. W. Goodman, "Gain optimization in switches based on semiconductor optical amplifiers," J. Lightwave Technol. **13**, 598–605 (1995).
30. D. Derickson, *Fiber Optic Test and Measurement* (Prentice Hall, 1998).
31. G. P. Agrawal, *Fiber-Optic Communication Systems*, 3rd ed. (Wiley, 2002).
32. O. Liboiron-Ladouceur, K. Bergman, M. Boroditsky, and M. Brodsky, "Polarization-dependent gain in SOA-based optical multistage interconnection networks," J. Lightwave Technol. **24**, 3959–3967 (2006).